



Numerical Study of Frictional Drag Reduction Using Micro-Bubbles in a Vertical Couette-Taylor System



Seyed Morteza Javadpour ^a, Reza Maryami ^b, Erfan Kadivar ^c

Manuscript submitted: 27 January 2022, Manuscript revised: 18 February 2022, Accepted for publication: 05 March 2022

Corresponding Author ^a



Keywords

Couette-Taylor system;
discrete-phase model;
drag reduction;
friction drag;
micro-bubbles;

Abstract

In this work, we numerically study the reduction of frictional drag in a vertical Couette-Taylor system by using micro-bubbles. The silicon flow is in the annular gap between two concentric cylinders as the internal cylinder is rotating while the outer cylinder is stationary. Taylor vortices are formed between the cylinders and the rotational Reynolds number also varies from 700 to 4500. The carrier flow is silicone while air bubbles are constantly injected into the carrier phase at the bottom of cylinders and rise through the flow. By employing a discrete phase model and Euler-Lagrange approach, we investigate a two-phase turbulent flow. In this way, we study the distribution of the bubbles through the flow, which is acquired using numerical modeling. Our numerical results are in good agreement with the experimentally reported data for different values of Reynolds numbers. We also investigate the effect of injected air with a constant flow rate on the skin friction drag and on the drag coefficient ratio. Our numerical results illustrate a reduction of drag about 36% when microbubbles are injected into the system. This reduction can be achieved by the effect of the bubbles on the density of the fluid and transformed momentum.

International Journal of Physical Sciences and Engineering © 2022.

This is an open access article under the CC BY-NC-ND license

(<https://creativecommons.org/licenses/by-nc-nd/4.0/>).

Contents

Abstract.....	50
1 Introduction	51
2 Materials and Methods.....	53
3 Geometry and Numerical Procedure.....	56
4 Results and Discussions	58
5 Conclusion.....	63

^a Department of Mechanical Engineering, University of Gonabad, Gonabad, Iran

^b Department of Mechanical Engineering, University of Yazd, Yazd, Iran

^c Department of Physics, Shiraz University of Technology, Shiraz, Iran

References.....	65
Biography of Authors.....	67

1 Introduction

Multiphase flow is an interesting branch of fluid mechanics. Studying different passive and active control methods to reduce the friction drag and increase the efficiency of a system subject to save energy are important topics due to practical applications (such as ships, submarines, reactors, turbomachinery, pipelines, etc.) as well as due to theoretical studies. In fact, a significant part of the energy is spent to overcome the resistance forces acting on a solid surface due to fluid flow which is called drag force. Drag force is a frictional force that dissipates energy in the system. In general, friction, pressure, and waveforms are three kinds of drag force. The friction force has the highest effect on energy losses. Therefore, in recent years, a large number of research efforts have been focused on drag reduction and energy saving. In other words, over the last decades, a series of experimental and numerical studies have been performed to study the reduction of drag. Some of the efficient methods used in previous investigations to reduce skin friction are micro-bubbles, surface modification using hydrophobic materials, micro vortex generators, injection, and suction methods, etc. Drag reduction using microbubbles injected into boundary layers has been studied by different researchers in practical applications, because of its simple usage, low cost, and no environmental pollution. In this way, microbubbles are injected around the submerged and floating body near the wall surface in order to manipulate the boundary layer and change the density of the fluid and transform the momentum.

The first empirical research on drag reduction was carried out by McCormick and Bhattacharyya who studied experimentally drag reduction using gas bubbles (McCORMICK & Bhattacharyya, 1973). Their experimental results show that the velocity of the model increases when the rate of hydrogen bubbles increases. Bogdevich et al. have experimentally investigated the effect of gas concentration on the viscous drag reduction on a flat-plate turbulent boundary layer (Bogdevich & Maluga, 1976; Bogdevich et al., 1977). The bubbles have been produced using porous plates when air passes through them. Their experimental results indicate that the concentration of bubbles near the wall is an important factor in viscous drag reduction. They also found that the best results of drag reduction were acquired when the concentration of bubbles reached a certain amount of accumulation. Madavan et al. have experimentally studied the influence of carrier flow speed and buoyancy force on the viscous drag reduction (Madavan et al., 1984). Their experimental setup consists of flat plates mounted horizontally in a water tunnel with a rectangular test section. Skin friction drag was measured using skin friction integrated over the entire the section, and local skin friction as well. Their experimental results indicate that the drag reduction decreases at a higher velocity for a certain rate of air bubbles. In addition, the viscous drag reduction on the upper wall is much larger than the lower wall at low speeds.

Lance and Bataille have experimentally studied the isotropic turbulence in a vertical channel (Lance & Bataille, 1991). Their results illustrate that the isotropy turbulence is independent of the void fraction. Moreover, the higher frequency energy of the spectra without bubbles is lower than with a void fraction of 1.9 %. However, the opposite trend was observed in the lower frequency range. Kodama et al. (2000), have performed experiments by using microbubbles in a water channel flow. The bubbles have been generated using a porous plate, which was located on the upper wall of the channel. Their experimental results show that the skin friction decreases by increasing the void fraction.

Xu et al. (2002), have carried out direct numerical simulation (DNS) by applying the force-coupling method (FCM) to simulate the presence of bubbles and their effects on the flow. They have found that for large bubbles, an initial transient drag reduction occurs when the air bubble disperses into the flow. Lu et al. (2005), have investigated the effect of large bubbles which were injected near the walls of the minimum turbulent channel on the skin friction. They have applied DNS and detected a significant reduction of the skin friction by suppression of streamwise vortices due to deformable bubbles. Kadivar et al. (2018,2019), have developed a passive control method called cavitating-bubble generators (CGs) to suppress the cavitation instabilities of the unsteady cloud cavitation at the high Reynolds numbers. Their results indicate that the CGs can generate a form of cavitating vortex which can influence the dynamics of the cavitation. They have also found that proper size and position of CGs on the suction side of a hydrofoil can change the mechanism of

unsteady cloud cavitation to quasi-steady cavitation and increase the hydrodynamic efficiency of the hydrofoil.

The effect of bubble size on micro-bubble drag reduction has been experimentally studied by Shen et al. (2006). In this work, nitrogen gas was applied to force flow through a slot injector located in the plate beneath the boundary layer of the tunnel test section. Their results indicate that microbubble drag reduction depends on the volumetric gas flow rate and the static pressure in the boundary layer. In contrast, this behavior was essentially independent of the size of the micro-bubbles. Skin friction reduction using bubbles has been experimentally investigated in a horizontal rectangular turbulent channel by Murai et al. (2007). The results indicate that bubbly drag reduction has much relevance to the shear layer. They have also investigated the relationship between variations of skin friction and bubble size. They reported that the skin friction decreases independently of the flow speed when bubbles are sufficiently larger than the boundary layer thickness.

The advantage of the Couette-Taylor system (CT) is a closed system and thus has a well-defined energy balance in analogy with the Rayleigh-Be'nard system (Lathrop et al., 1992, Eckhardt et al., 2007, Ahlers et al., 2009). In addition, CT flow can give the possibility of measuring global torque and gas volume fraction with good accuracy. In CT systems fluid flows between two cylinders one of which is kept fixed and another one rotates around its axis. By increasing the angular velocity of the inner cylinder, Taylor-vortices are formed between two cylinders (see Figure 1b). The first research on Couette-Taylor flow was carried out by Couette (Couette, 1890); Mallock (1896); Taylor (1923). The experimental and numerical studies indicate that the stability and flow pattern of Couette-Taylor flow depends on axial flow (Cornish, 1933; Goldstein, 1937; Chung & Astill, 1977, Takeuchi & Jankowski, 1981, Lueptow et al., 1992; Shiomi et al., 1993; Atkhen et al., 2000; Hubacz & Wroński, 2004).

Bubbly CT flow has been experimentally and numerically studied in recent years (Murai et al., 2005; Murai et al., 2008; Mehel et al., 2007; Van der Berg et al., 2005; Van der Berg et al., 2007; Van Gils et al., 2013; Maryami et al., 2014; Maryami et al., 2015; Maryami et al., 2015; Maryami et al., 2016; Sugiyam et al., 2008). The influence of solid particles and microbubbles on the viscous drag reduction in the turbulence CT flow has been experimentally and numerically studied by Van der Berg et al. (2005, 2007). They have also investigated the effect of bubble size and Reynolds number on viscous drag reduction. By using Eulerian-Lagrangian model with point-force coupling, the effect of microbubbles on a Taylor-Couette flow in the wavy vortex flow regime has been numerically investigated by Djeridi et al. (2004). Their numerical results indicate that the strength of lift force is an important factor for the bubble mean concentration profiles.

In the present work, by using the Eulerian-Lagrangian approach, we will numerically study the effect of microbubbles on drag reduction in the vertical CT system. In order to validate our numerical results, the geometry and flow characteristics were chosen similar to those chosen by Murai et al. (2008), which are listed in Table 1. Therefore, according to the variation range of angular velocity of the inner cylinder, flow is turbulent and microbubbles are injected into the flow at the bottom of the system. In this study, the simulation of two-phase flow in the annulus gap between coaxial cylinders is performed using a discrete phase model (DPM). Moreover, the model is applied to simulate turbulent CT flow and Reynolds's stresses. The effect of microbubbles on the drag reduction via acted torque on the system and drag coefficient is also investigated.

Table 1
Experimental conditions (Murai et al., 2008)

Experimental conditions	
Inner cylinder radius	$R_1 = 60mm$
Outer cylinder radius	$R_2 = 72mm$
Height of fluid-filled	$L_1 = 240mm$
The average diameter of bubbles	$0.5mm$
Density of fluid	$\rho_l = 915kg / m^3(at298k)$
Kinematic viscosity of the fluid	$\nu_l = 5 \times 10^{-6} m^2 / s(at298k)$
Airflow rate	$0 \leq Q_a \leq 1.67 \times 10^{-6} m^3 / s$
Angular velocity of the inner cylinder	$4.861 \leq \omega \leq 31.25$

Rotational Reynolds number	$700 \leq \text{Re}_\omega \leq 4500$
Taylor number	$98 \times 10^3 \leq Ta \leq 40.5 \times 10^5$

2 Materials and Methods

The computational fluid dynamics approach for the numerical simulation of the gas-fluid interface can be categorized into two groups: 1- the Eulerian-Eulerian approach or two-fluid model, and 2- the Eulerian-Lagrangian approach or discrete phase model (DPM). In the last one (DPM), the fluid phase is solved using the Navier-Stokes equations, and the motion of the bubble phase is solved using Newton's second law of motion. The model governing equations for CT flow are briefly explained in the form of tensor notations as follow: By assuming incompressibility of the flow, the conversation of mass reads:

$$\frac{\partial \rho_l}{\partial t} + \frac{\partial}{\partial x_i} (\rho_l u_i) = 0 \quad (1)$$

and by assuming constant fluid properties and incompressible Newtonian fluid, the conversation of momentum leads to:

$$\frac{\partial (\rho_l u_i)}{\partial t} + \frac{\partial}{\partial x_i} (\rho_l u_i u_j) = -\frac{\partial p}{\partial x_i} + \frac{\partial}{\partial x_j} \left[\mu_l \left(\frac{\partial u_i}{\partial x_j} + \frac{\partial u_j}{\partial x_i} - \frac{2}{3} \delta_{ij} \frac{\partial u_k}{\partial x_k} \right) \right] + \frac{\partial}{\partial x_j} (-\rho_l \overline{u'_i u'_j}) \quad (2)$$

where u_i is velocity, p is pressure, and ρ_l is density. To solve Navier-Stokes equations including turbulent motion, statistical methods should be extended in which the turbulent motion is computed by means of time-averaged quantities instead of instantaneous quantities. The most widely used approach for many engineering applications that fulfills the required levels of accuracy and efficiency calls Reynolds-averaged Navier-Stokes (RANS) equations. The Boussinesq hypothesis is used to relate the Reynolds stresses to the mean velocity gradients using an eddy viscosity. Therefore, by applying the $k-\omega$ model, Reynolds's stresses term $(-\rho_l \overline{u'_i u'_j})$ in momentum equations can be read as

$$(-\rho_l \overline{u'_i u'_j}) = \mu_l \left(\frac{\partial u_i}{\partial x_j} + \frac{\partial u_j}{\partial x_i} \right) - \frac{2}{3} \left(\rho_l k + \mu_l \frac{\partial u_k}{\partial x_k} \right) \delta_{ij} \quad (3)$$

where μ_l is eddy viscosity? The standard $k-\omega$ model is a semi-empirical model like the standard $k-\varepsilon$ model. This model is proposed by Wilcox (2006). In this model, the transport equations for the turbulence kinetic energy k and the specific dissipation rate ω write as follows:

$$\frac{\partial}{\partial t} (\rho_l k) + \frac{\partial}{\partial x_j} (\rho_l u_j k) = P - C_{\mu_l} \rho_l \omega k + \frac{\partial}{\partial x_j} \left[(\mu_l + \sigma_k \mu_l) \frac{\partial k}{\partial x_j} \right] \quad (4)$$

$$\frac{\partial}{\partial t} (\rho_l \omega) + \frac{\partial}{\partial x_j} (\rho_l u_j \omega) = \frac{\gamma \rho_l}{\mu_t} P - \beta \rho_l \omega^2 + \frac{\partial}{\partial x_j} \left[(\mu_l + \sigma_\omega \mu_l) \frac{\partial \omega}{\partial x_j} \right] + (1 - F_1) 2 \rho_l \sigma_\omega \frac{1}{\omega} \frac{\partial \kappa}{\partial x_j} \frac{\partial \omega}{\partial x_j} \quad (5)$$

The constant and variable parameters used in the above equations are mentioned by Wilcox (2006). To investigate changes of shear stress in CT flow, flow temperature variations are assumed to be below.

Therefore when the two-phase turbulent flow is solved, flow temperature has a constant amount of 298k. The gas bubble is treated as a discrete phase. The bubble trajectory is calculated by integrating the force balance on it which is written in a Lagrangian reference frame. The bubble of motion which equates the bubble inertia with the forces acting on the bubble reads as

$$\frac{du_b}{dt} = F_D(u_i - u_b) + \frac{g(\rho_b - \rho_l)}{\rho_b} \quad (6)$$

where u_i is the fluid velocity, u_b is bubble velocity, and $F_D(u_i - u_b)$ is the drag force per unit bubble mass and F_D is defined by

$$F_D = \frac{18\mu_l C_D \text{Re}}{\rho_b d_b^2} \frac{C_D \text{Re}}{24} \quad (7)$$

d_b is bubble diameter, ρ_b is bubble density, and Re is relative Reynolds number. The variable parameters used in the above equation are as follows:

$$\text{Re} \equiv \frac{\rho_l d_b |u_b - u_i|}{\mu_l} \quad (8)$$

$$C_D = C_{D,sphere}(1 + 2.632y) \quad (9)$$

$$C_{D,sphere} = \begin{cases} 0.242 \dots \dots \dots \text{Re} > 1000 \\ \frac{24}{\text{Re}} \left(1 + \frac{1}{6} \text{Re}^{2/3} \right) \dots \text{Re} \leq 1000 \end{cases} \quad (10)$$

In Eq. 9 y is the bubble distortion, as determined by the solution of

$$\frac{d^2 y}{dt^2} = \frac{C_F \rho_b u_b^2}{C_g \rho_l r_b^2} - \frac{C_k \sigma_b}{\rho_l r_b^3} y - \frac{C_d \mu_l}{\rho_l r_b^2} \frac{dy}{dt} \quad (11)$$

$$C_k = 8, C_d = 5, C_F = 1/3, C_g = 0.5$$

$$C_k = 8, C_d = 5, C_F = 1/3, C_g = 0.5$$

The rotational Reynolds number is defined based on the radius of the internal cylinder as this cylinder is rotating in this work. So

$$\text{Re}_\omega = \frac{R_1 \dot{\alpha} \rho}{\nu_l} \quad (12)$$

where ν_l is the kinematic viscosity of pure silicon oil, i.e. silicon oil without micro bubbles. In order to use pure fluid viscosity or mixture viscosity, there are two scenarios. The first one is that the two-phase flow in CT system is considerably inhomogeneous. Therefore, the original kinematic viscosity of fluid can be used to define rotational Reynolds number (Murai et al., 2008). The second one is that bubbles affect the physical properties of the fluid, thus mixture viscosity should be applied to calculate the rotational Reynolds number (Batchelor & Batchelor, 2000; Rust & Manga, 2002). The formation of Taylor vortices in CT flow depends on rotational Reynolds number and air-gap length. These parameters are included in the Taylor number that is defined by

$$Ta = \text{Re}_\omega^2 \frac{\delta}{R_1} \quad (13)$$

In the present research, the maximum rotational Reynolds number is 4500 (see Table 1), so according to identified five different regions for CT flow by Murai et al. (2008), the flow region is turbulent wavy vortex flow (TWTF). On the other hand, in a simple CT flow Taylor vortices appear in the annulus gap when Taylor number reaches to critical Taylor number ($Ta_{cr} = 1.7 \times 10^3$) (Gazley Jr, 1958). Since in this work minimum Taylor number is greater than the critical Taylor number, the Taylor vortices undoubtedly appear inflow. In the single-phase CT flow, the integrated force can be computed by integrating shear stress acting on the inner cylinder surface as follow:

$$F = \int \tau_w dA = 2\pi \int_0^{L_1} \tau_w R_1(L) dL \quad (14)$$

In the above equation τ_w is wall shear stress and is computed by

$$\tau_w = \mu_l \frac{du_i}{dx_i} \quad (15)$$

It should be noted that only the component of the wall shear stress vector in planes perpendicular to the axis of the cylinder affects the rotational velocity of the inner cylinder. The other component of this stress with a vector lying in planes that extend through the axis of the cylinder can be ignored in order to it does not directly affect the rotational of the inner cylinder. Therefore, the torque acting on the inner cylinder is calculated by

$$T = 2\pi \int_0^{L_1} \tau_w R_1^2(L) dL \quad (16)$$

By calculating τ_w drag coefficient yielded

$$C_f = \frac{2\tau_w}{\rho_l (R_1 \omega)^2} \quad (17)$$

To study the effect of injected microbubbles on frictional drag reduction in CT flow, the ratio of friction coefficient is driven using this equation

$$\eta = 1 - \frac{C_f}{C_{f_0}} \quad (18)$$

In order to compare reduced power in the presence of microbubbles with the necessary power to inject air into the flow a dimensionless parameter which is called power gain is used. This parameter is defined by

$$G = \frac{(T_0 - T) \omega}{\rho_l g L_1 Q_a} \quad (19)$$

In Eq. 19 the numerator illustrates the reduced power when microbubbles are injected into CT flow and the denominator represents the necessary power to inject air into CT flow. In the last two equations subscript "0" represents the single-phase flow condition.

3 Geometry and Numerical Procedure

Figure 1 a shows a schematic two-dimensional diagram of the geometry (simulated CT system) and flow when air bubbles are injected into the annulus gap between coaxial cylinders. The rotating inner cylinder has an outer diameter of 120 mm and the fixed outer cylinder has an inner diameter of 144 mm. In order to have enough bubbles between cylinders, the gap between cylinders was selected 12 mm which is 20 times greater than the bubble diameter. The effective height between two cylinders, L_1 , was selected 240 mm and the space between cylinders is filled by silicon oil to give enough motion time and space to the bubbles in the flow. Air is injected at the bottom of the cylinders into the main flow through four holes. The holes' positions were precisely selected to have homogeneous bubbles in the system.

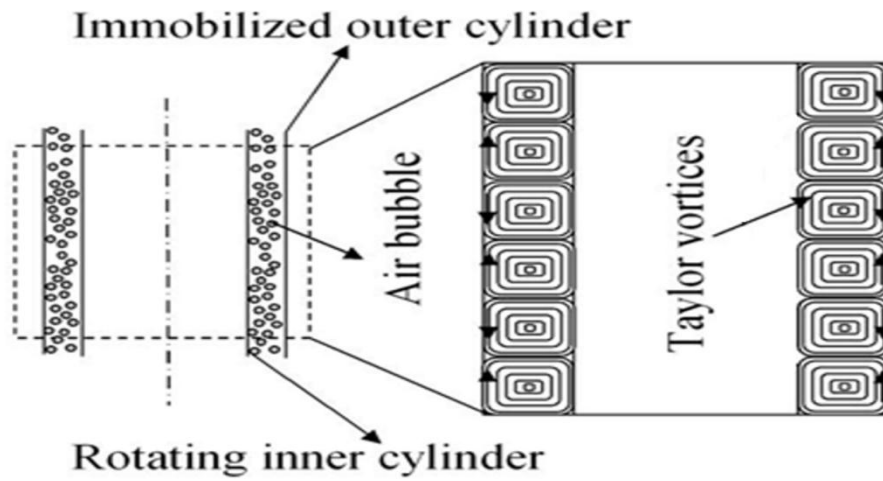


Figure 1. Schematic of the vertical Couette–Taylor flow system a) geometry characteristics and bubbles pattern(left), b) schematic of Taylor-vortices(right).

If the internal cylinder rotates with constant angular velocity, Couette-flow or Taylor-vortices is depending on the angular velocity. When the angular velocity is less than a critical value, the three-dimensional vortices called Taylor-vortices (see Figure 1b) are not formed and the flow is Couette-flow. It means that the Taylor-vortices are formed when the angular velocity increases and passes a critical value. Taylor-vortices keep their shape until a certain rotational speed is greater than the critical speed of rotation. By increasing the rotational speed of the inner cylinder, Taylor-vortices are distorted and then disappeared. Hence, the flow in the annulus gap becomes fully turbulent.

To simulate the flow in the vertical CT system, first the flow area is meshed as shown in Figure 2, i.e. a three-dimensional mesh is produced. The finite volume method is employed to discrete the governing equations. Coupled procedure method is used to solve the momentum equations and tracing the bubbles path as well. To provide a good tool in order to simulate the two- phase flow, DPM and Euler-Lagrange approaches are employed.

The boundary conditions in the CT flow system are as follows:

- No slip conditions are used for all velocity components of the flow.
- At the injectors' inlets, the air to produce bubbles with a specified volume flow rate or pressure is assumed.
- Outlet pressure is equal to surrounding pressure and the top of the CT system is open.

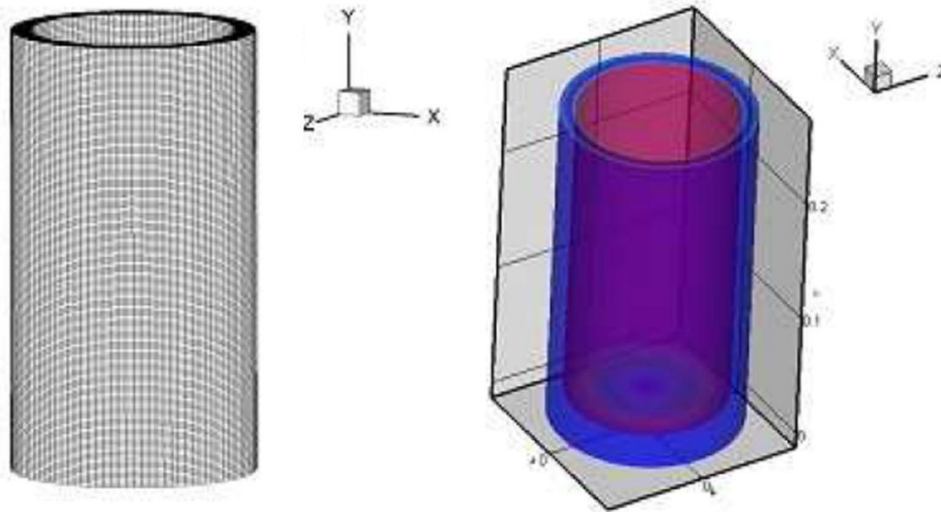


Figure 2. (left) typical three-dimensional grid, (right) geometry of vertical CT system

In order to investigate the grid independency of the results, at five different nodes ($N_1 = 180000$, $N_2 = 330000$, $N_3 = 550000$, $N_4 = 800000$, $N_5 = 900000$ nodes) and for the case $Q_a = 0.67 \times 10^{-6} \text{ m}^3 / \text{s}$, $Re_\omega = 2800$ the numerical drag coefficient is calculated and is compared with $C_{f_{exp}} = 5.8 \times 10^{-3}$ which has been acquired by experimental method (Hubacz & Wroński, 2004). As shown in Table 2, the difference between numerical and experimental drag coefficients in the last two nodes is small. Moreover, it is observed that minimum changes of numerical drag coefficient exist between the last two grids, so a grid with $N_4 = 800000$ nodes is used in this research.

Table 2

Variations of $C_{f_{num}}$ at five different nodes for the case $Q_a = 0.67 \times 10^{-6} \text{ m}^3 / \text{s}$, $Re_\omega = 2800$ and comparison of this coefficient with $C_{f_{exp}} = 5.8 \times 10^{-3}$ which has been acquired by experimental method (Murai et al., 2008)

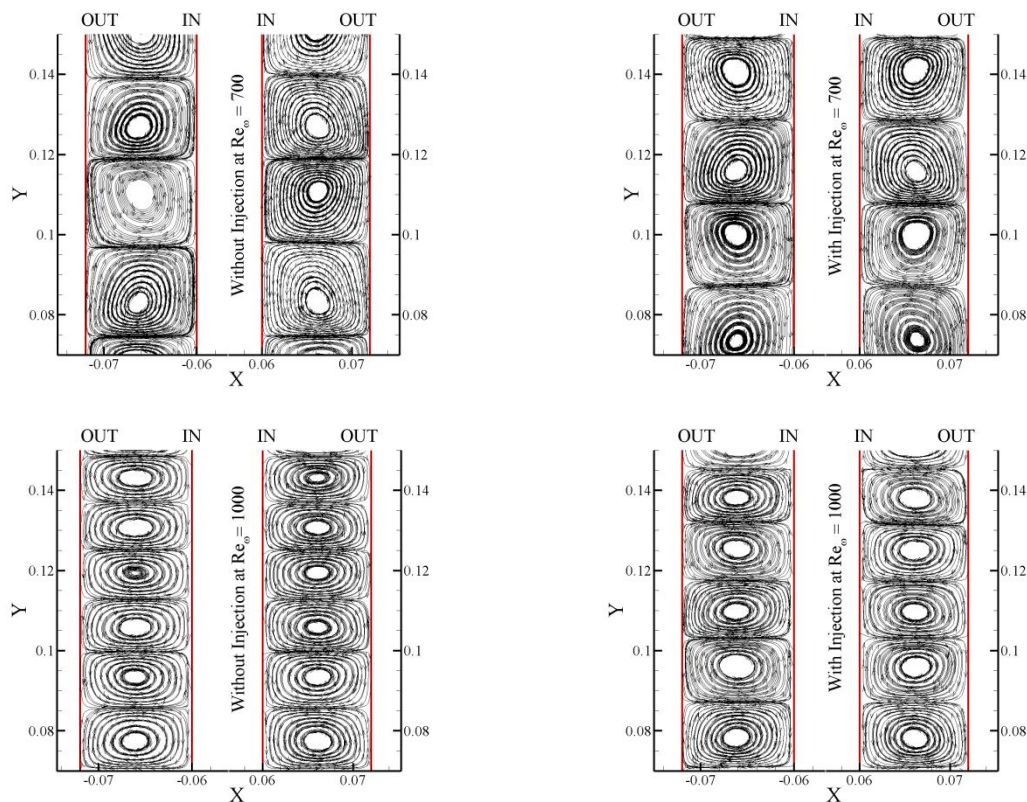
Variations of $C_{f_{num}}$ at five different nodes for the case $Q_a = 0.67 \times 10^{-6} \text{ m}^3 / \text{s}$, $Re_\omega = 2800$ and comparison of this coefficient with $C_{f_{exp}} = 5.8 \times 10^{-3}$ which has been acquired by experimental method			
Node	$C_{f_{num}}$	$e_1 = \frac{C_{f_{exp}} - C_{f_{num}}}{C_{f_{exp}}} \times 100$	$e_2 = \frac{C_{f_{numj}} - C_{f_{numj-1}}}{C_{f_{numj}}} \times 100$
$N_1 = 180000$	0.0055	5.172%	7.27%
$N_2 = 330000$	0.0059	1.724%	3.39%
$N_3 = 550000$	0.0057	0.993%	1.75%
$N_4 = 800000$	0.0056	1.724%	0%
$N_5 = 900000$	0.0056	1.724%	

4 Results and Discussions

In order to investigate the flow characteristics, the acquired flow patterns for four rotational Reynolds numbers ($Re_\omega = 700, Re_\omega = 1000, Re_\omega = 1800, Re_\omega = 4500$) and in cases with and without injection are visualized as shown in Fig. 3. The results illustrate that injection of microbubbles into the annulus gap leads to reduction of Taylor vortices number along the axis of cylinders. In fact, in the presence of microbubbles in CT flow, Taylor vortices are elongated (i.e. original wavelength of each pair of vortices expands) in the cylinder-axial direction which corresponds to the decrease in the number of Taylor vortices. Since the appearance of Taylor vortices and their movement along the cylinder's axis provides momentum transfer and increases it, the elongation causes the reduction in momentum transfer. These results are in good agreement with those found by [Murai et al. \(2008\)](#), experimentally.

The elongation of Taylor vortices is due to the produced thin air layer between vortices and the inner cylinder surface. In fact, when the inner cylinder is rotated, the centrifugal force affects injected air bubble's inflow and leads to their movement toward the inner cylinder surface. The accumulation of air bubbles in this area creates bubble clouds that are coalesced together and form a thin air layer. By moving air bubbles toward the inner cylinder, fluid elements move in the adverse direction (i.e. toward the outer cylinder) and the necessary space to form vortices in the cylinder-radius direction in the annulus gap is decreased. Consequently, three-dimensional fluctuations of flow (Taylor vortices) are expanded along the axis of cylinders.

It should be noted that creating a thin air layer between Taylor vortices and rotating surface in addition to reduction of momentum transfer by elongating vortices leads to reduction of the average density of the fluid and increasing effective viscosity of the fluid near this surface. In this case, the convection of the small shear stresses from turbulent portions of the boundary layer toward the rotating surface is decreased. Therefore, the flow close to the surface becomes laminar and the skin friction drag is reduced.



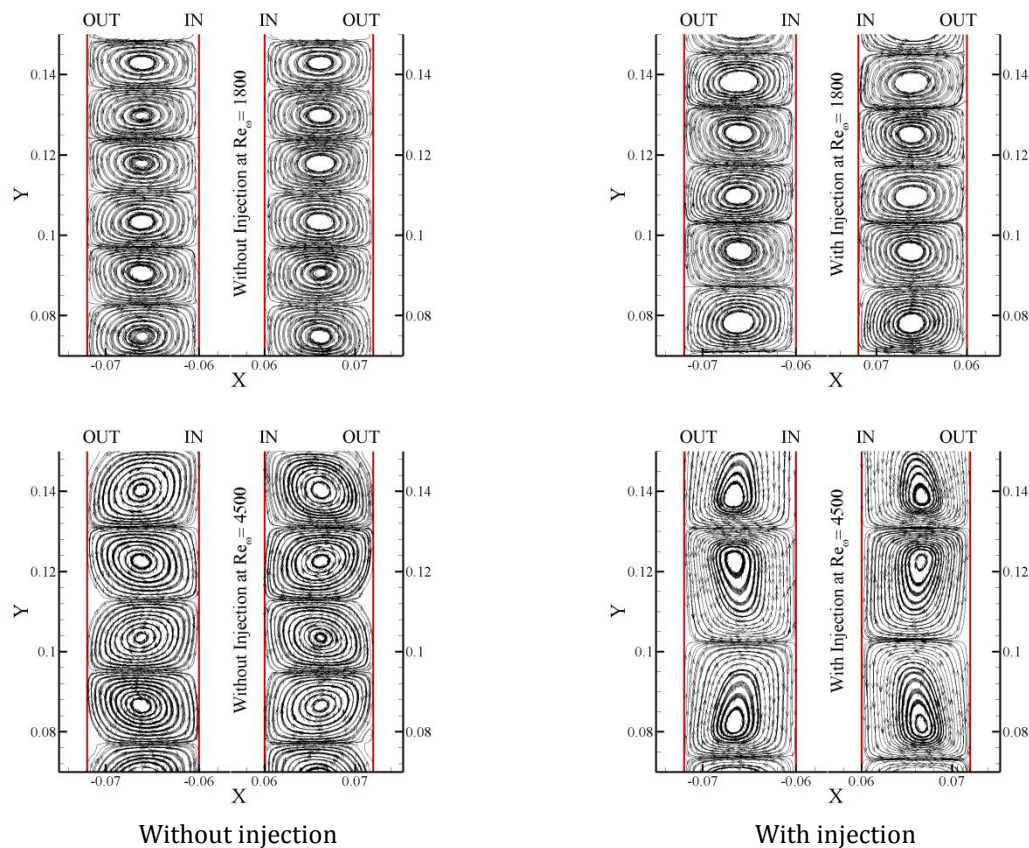


Figure 3. Flow pattern comparison on the plane passing through the axis (plane $z = 0$) for the case $Q_a = 0.67 \times 10^{-6} \text{ m}^3/\text{s}$ and indifferent Re_ω

Figure 4 illustrates the distribution of bubbles after their injection into the system at different rotational Reynolds numbers. The total appearance time of bubbles in the whole of the test section is 5.6 s and the colored bar represents the position of bubbles in each time. It is observed that in the low rotational Reynolds number bubbles are dispersed everywhere in the fluid from the bottom to the top of the test section. By increasing this dimensionless number bubbles accumulate at the bottom parts of the system. This relates to the enhancement of rotational speed and the effect of centrifugal force on the bubbles.

Figure 5a shows variations of drag coefficient and Figure 5b shows changes of drag coefficient ratio. In these figures, the mentioned variations for numerical and experimental methods are based on rotational Reynolds number changes, in various airflow rates. The results illustrate that by increasing the rotational Reynolds number, in each airflow rate, the drag coefficient is decreased. However, in the case of supplied largest air flow rate ($Q_a = 1.67 \times 10^{-6} \text{ m}^3/\text{s}$) the changes of drag coefficient occur non-monotonically. Murai et al. (2008), believed that changes in flow pattern because of the reaction between two-phase that corresponds to bulk void fraction changes, maybe the reason for this variation.

Figure 5b shows that in each airflow rate, rotational Reynolds number increase leads to reduction of drag coefficient ratio, i.e. the effect of microbubbles on drag reduction is decreased in this condition. As shown in Fig. 5a, decreasing the difference between drag coefficients in cases with and without injection is evidence of this issue when the rotational Reynolds number is increased. The reason for this is the increasing effect of centrifugal force acting on microbubbles that leads to resting the bubbles at horizontal levels in the air gap and do not more travel upward streamwise direction as shown in Figure 4. In this condition, bubbles do not spread everywhere in inflow and they could not affect the inertial force or transfer momentum (Kim & Cleaver, 1995; Farfán et al., 2021; Arauz et al., 2016).

On the other hand, the centrifugal force causes the accumulation of bubbles and creates bubble clouds that are located between Taylor vortices and near the inner cylinder surface as mentioned before (see Figure 6). Since by increasing rotational Reynolds number, the centrifugal force becomes stronger and a further number of bubbles move toward the inner cylinder, the bubble clouds are greater than created clouds in low rotational Reynolds number. In such a case, clouds affect the motion of Taylor vortices and lead to increasing their movement and also momentum transfer increase. Moreover, great bubble clouds effectively destroy created boundary layer on cylindrical surfaces, so by amplifying resistance shear forces skin friction is increased.

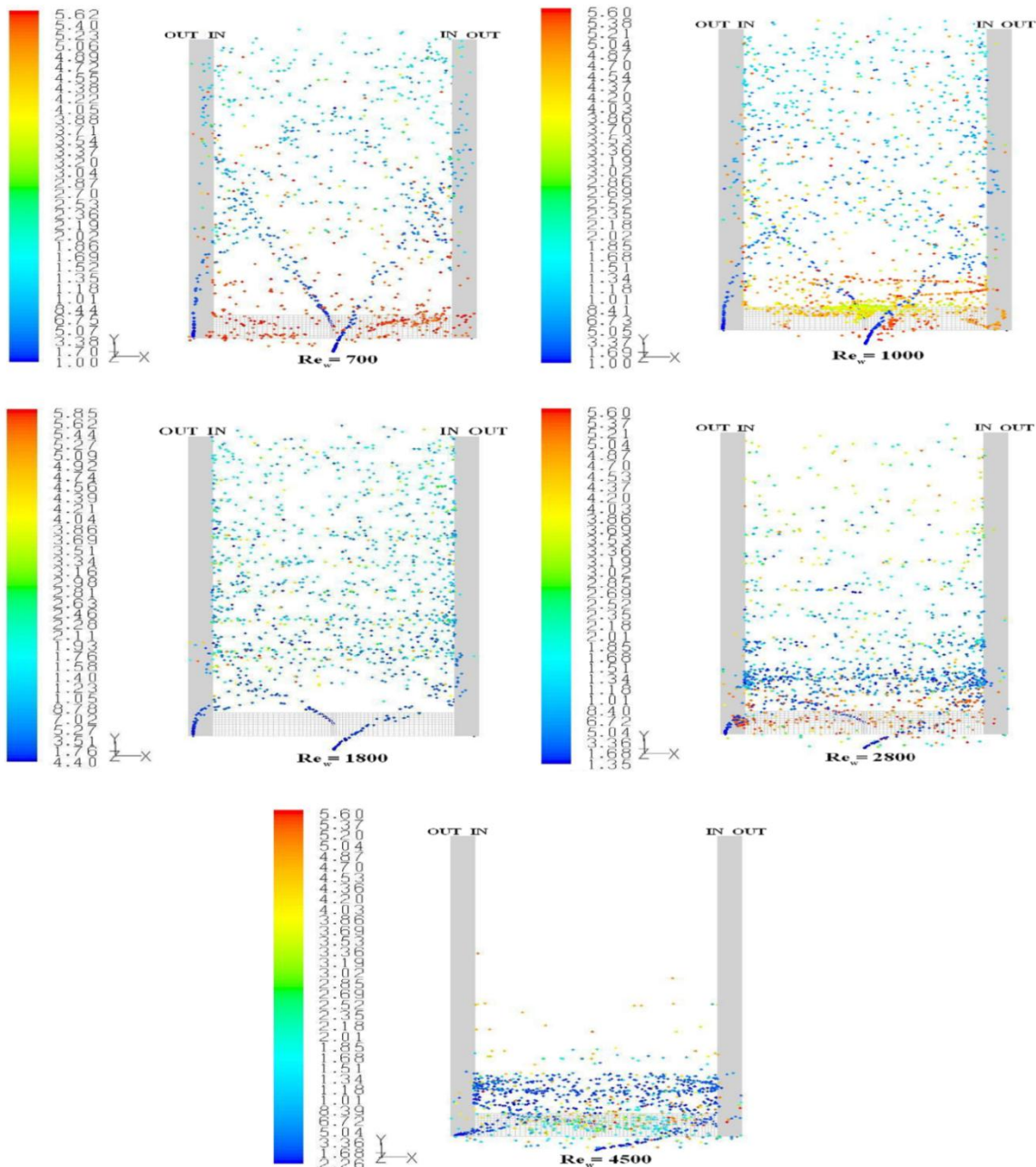


Figure 4. Comparison of bubbles distribution in CT system for the case $Q_a = 0.67 \times 10^{-6} \text{ m}^3 / \text{s}$ and in different values of Re_ω .

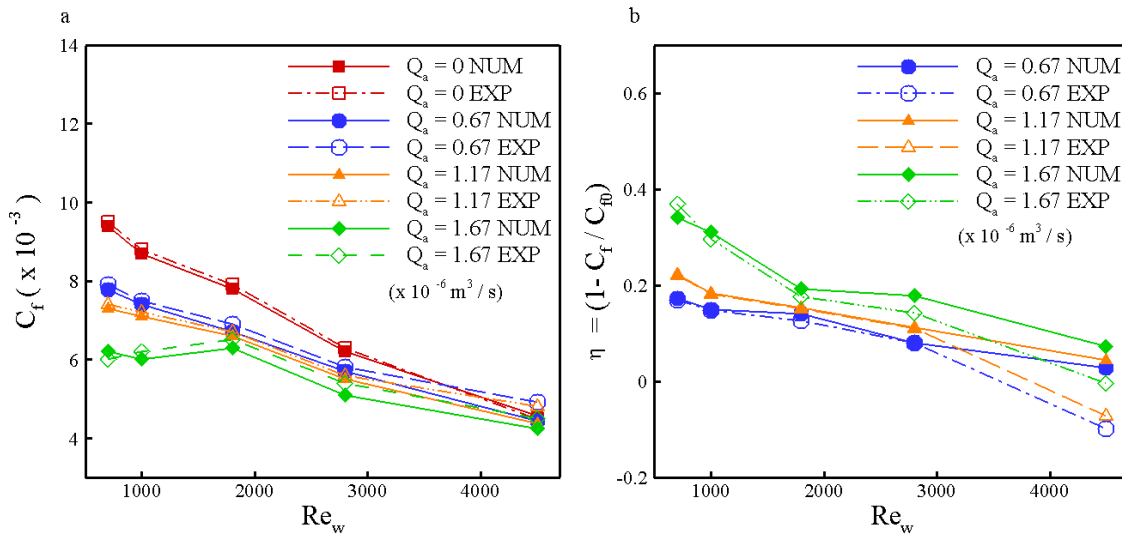


Figure 5. Variations of C_f vs. Re_w shown in (a) and variation of η vs. Re_w shown in (b) for different airflow rates.

In addition to mentioned mechanisms, Murai et al. (2008), supposed that coalescing bubbles occur into Taylor vortex cores when bubbles travel to the center of Taylor vortices owing to increasing rotational Reynolds number. In this condition, each vortex can survive and enhance momentum transfer. In all cases, enhancement of flow turbulence by additional produced momentum transfer is more important factor to justify the decreasing effect of microbubbles on drag reduction.

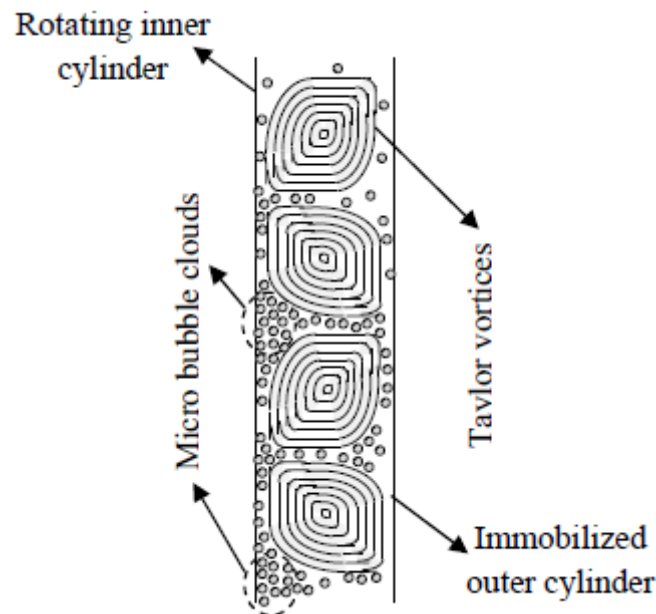


Figure 6. Schematic of Taylor vortices appearance and microbubbles accumulation between vortices

The effect of air flow rate on the drag coefficient and drag coefficient ratio at different rotational Reynolds numbers is also shown in Figure 7. The results indicate that in each rotational Reynolds number, increasing airflow rate leads to drag coefficient decrease as shown in Figure 7a. In this condition, Figure 7b shows that the drag coefficient ratio is increased and in the highest case this ratio reaches 36%. Increasing the upward

velocity of bubbles is a reason for these variations. In this case, bubbles have remained singly inflow and lesser bubbles have coalesced together in order that the effect of centrifugal force on bubbles is decreased. When bubbles are dispersed singly in the flow, the better affect fluctuations of flow and also reduce momentum transfer. In fact, mono microbubbles absorb the energy of flow fluctuations by their deformability while bubble clouds do not absorb this energy in this condition. Moreover, the increasing upward velocity of bubbles causes bubbles to spread everywhere inflow and interact with all flow fluctuations, so reduction of momentum transfer is increased (Wu et al., 2007; Sayyaadi & Nematollahi, 2013).

To identify the difference between numerical and experimental drag coefficient, the variations of drag coefficient as a function of airflow rate and rotational Reynolds number is indicated in Table 3 in addition to Figure 5 and 7. The results show a maximum 9.6% difference between these two coefficients.

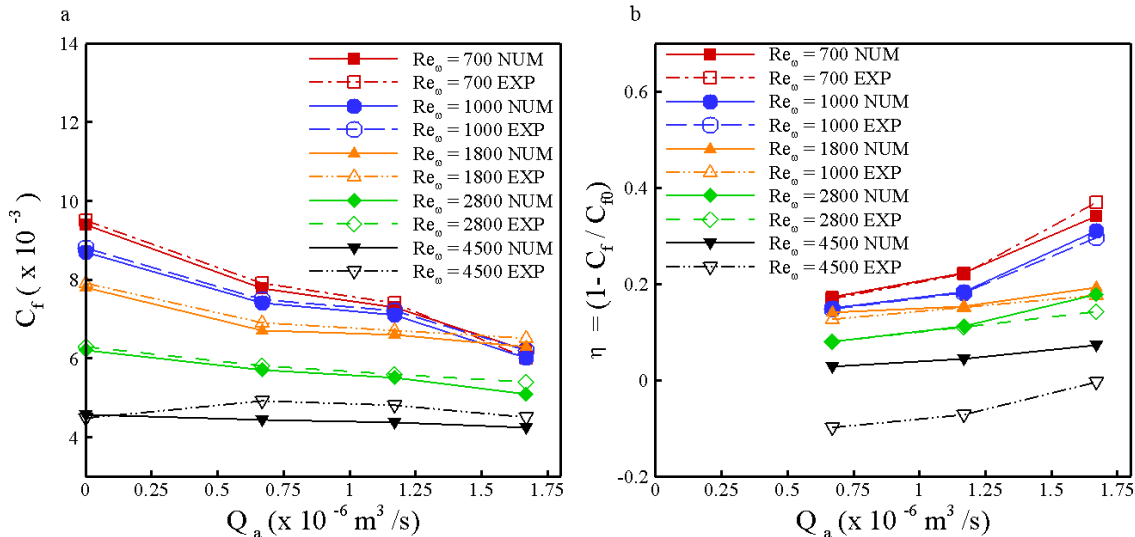


Figure 7. Variations of C_f and η vs. Q_a for different rotational Reynolds numbers

Table 3

Comparison of $C_f \times 10^{-3}$ which is acquired by numerical method (present work) and experimental method (Murai et al., 2008)

Comparison of $C_f \times 10^{-3}$ which is acquired by numerical method (present work) and experimental method												
Re_ω	$Q_a = 0 \times 10^{-6} m^3/s$			$Q_a = 0.67 \times 10^{-6} m^3/s$			$Q_a = 1.17 \times 10^{-6} m^3/s$			$Q_a = 1.67 \times 10^{-6} m^3/s$		
	$C_{f_{exp}}$	$C_{f_{num}}$	e%	$C_{f_{exp}}$	$C_{f_{num}}$	e%	$C_{f_{exp}}$	$C_{f_{num}}$	e%	$C_{f_{exp}}$	$C_{f_{num}}$	e%
700	9.5	9.4	1.052	7.9	7.8	1.51	7.4	7.3	1.35	6	6.2	3.33
1000	8.8	8.7	1.136	7.5	7.4	1.33	7.2	7.1	1.38	6.2	6	3.22
1800	7.9	7.8	1.265	6.9	6.7	2.89	6.7	6.6	1.50	6.5	6.3	3.07
2800	6.3	6.2	1.587	5.8	5.6	1.72	5.6	5.5	1.78	5.4	5.1	5.55
4500	4.48	4.56	1.785	4.92	4.43	9.96	4.8	4.36	9.16	4.5	4.23	6.00

Figure 8 shows changes of numerical and experimental power gain based on rotational Reynolds number in various airflow rates. The results illustrate that by increasing rotational Reynolds number, in each airflow rate, the acquired power gain by the experimental method (Murai et al., 2008), changes non-monotonically while numerical power gain is increased in this condition. In fact, it is observed that by increasing rotational Reynolds number up to 2800 experimental power gain is increased and in the range of $2800 < Re_\omega \leq 4500$ it is

decreased. Since in all range of rotational Reynolds number, the numerical power gain is greater than one, reduced power by injection of microbubbles is greater than necessary power to produce bubbles in the flow. Consequently, according to these results, the utilization of microbubbles is economical to reduce skin friction drag in the presence of CT flow. Although, the experimental results of power gain show that only at $Re_{\omega} \leq 4500$ power gain is greater than one and at $2800 < Re_{\omega} \leq 4500$ this factor is smaller than one. Therefore, the difference between experimental power gain and numerical power gain $2800 < Re_{\omega} \leq 4500$ is more as shown in Figure 8.

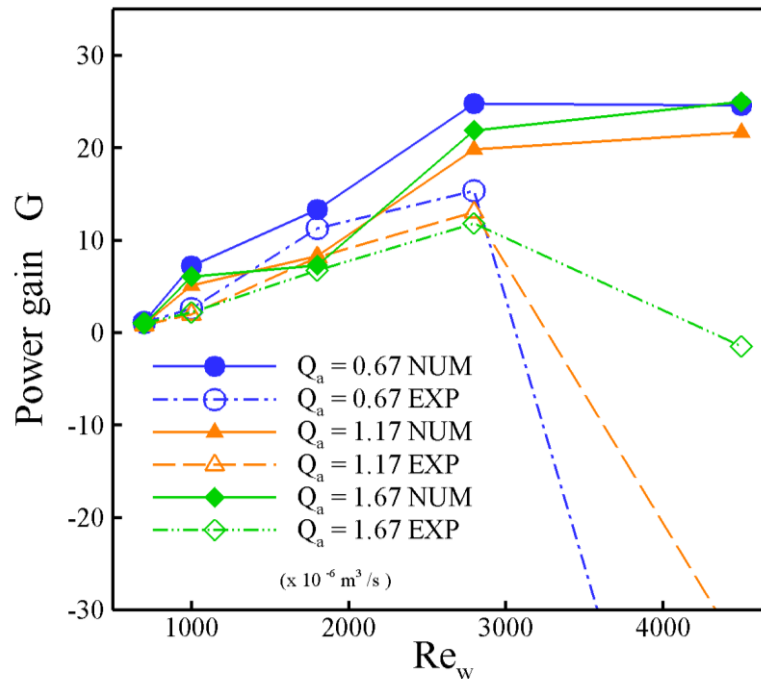


Figure 8. Variations of power gain vs. Re_{ω} for different airflow rates

5 Conclusion

In this work, the drag reduction due to the presence of micro in a vertical CT flow system bubbles has been numerically studied. Our suggested channel geometry consists of coaxial cylinders in which the inner cylinder rotates and the outer cylinder is stationary. The silicon oil phase flows through in the annulus gap between concentric cylinders and air bubbles are injected at the bottom of the system into the air gap. In the present study, the flow condition is turbulence, and Taylor vortices (three-dimensional fluctuations of flow) appear in all ranges of rotational Reynolds number. In order to investigate the effect of microbubbles on the drag reduction, $k-\omega$ and DPM models were used to simulate the turbulent flow in the CT flow. Our numerical results show that microbubble drag reduction depends on the variations of airflow rate and as well as on the rotational Reynolds number. In fact, it is observed that by increasing the airflow rate, the drag reduction increases and inversely increasing rotational Reynolds number leads to reduction of the microbubbles effect on the skin friction drag. In the present study, several mechanisms have been explained to justify the positive effects of microbubbles on drag reduction:

By producing a thin air layer between Taylor vortices and the rotating inner cylinder in the presence of microbubbles, the average density of fluid near the rotating surface decreases while its effective viscosity increases. In this case, the convection of shear stresses reduces from the turbulent region of the boundary

layer toward the rotating surface. This event leads to creating laminar flow in this area and reduction of drag. The elongation of Taylor vortices occurs along the axis of cylinders as the microbubbles are injected into flow. In this case, the number of vortices and also their movement in the cylinder axis direction decrease. This event leads to decreasing momentum transfer and flows turbulence.

Microbubbles interact with flow fluctuations and absorb the energy of fluctuations due to their elasticity. By reducing the energy of flow fluctuations, momentum transfer and flow turbulence decrease. On the other hand, there are a few scenarios to explain the reduction of microbubble's effect on skin friction decrease when rotational Reynolds number increases. In the first one, the accumulation of microbubbles in cores of the Taylor vortex leads to the survival of the vortices in the annulus gap and increasing momentum transfer. The second one is an accumulation of microbubbles close to the rotating surface and creating great bubble clouds that cause movement of Taylor vortices along with axis cylinders and increasing momentum transfer. And finally, the last one is bubbles remain in the horizontal level of flow and do not more travel upward in a streamwise direction. In this case, bubbles could not appear everywhere in the flow and affect flow fluctuations, so reduction of momentum transfer in the presence of microbubbles becomes less.

References

- Ahlers, G., Grossmann, S., & Lohse, D. (2009). Heat transfer and large scale dynamics in turbulent Rayleigh-Bénard convection. *Reviews of modern physics*, 81(2), 503.
- Arauz, W. M. S., Gamez, M. R., Perez, A. V., & Fernandez, M. C. (2016). Microgrids views from a geographic information system. *International Research Journal of Engineering, IT & Scientific Research*, 2(11), 57-65. Retrieved from <https://sloap.org/journals/index.php/irjeis/article/view/521>
- Atkhen, K., Fontaine, J., & Wesfreid, J. E. (2000). Highly turbulent Couette-Taylor bubbly flow patterns. *Journal of fluid mechanics*, 422, 55-68.
- Batchelor, C. K., & Batchelor, G. K. (2000). *An introduction to fluid dynamics*. Cambridge university press.
- Bogdevich, V. G., & Malyuga, A. G. (1976). The distribution of skin friction in a turbulent boundary layer of water beyond the location of gas injection. *Investigation of boundary layer control*. Thermophysics Institute Publishing, Novosibirsk, Siberia, 62.
- Bogdevich, V. G., Evseev, A. R., Malyuga, A. G., & Migirenko, G. S. (1977, January). Gas-saturation effect on near-wall turbulence characteristics. In *2nd Int. BHRA Fluid Drag Reduction Conf.:(United States)* (No. CONF-7708129-).
- Chung, K. C., & Astill, K. N. (1977). Hydrodynamic instability of viscous flow between rotating coaxial cylinders with fully developed axial flow. *Journal of Fluid Mechanics*, 81(4), 641-655.
- Cornish, R. J. (1933). Flow of water through fine clearances with relative motion of the boundaries. *Proceedings of the Royal Society of London. Series A, Containing Papers of a Mathematical and Physical Character*, 140(840), 227-240.
- Couette, M. (1890). *Etudes sur le frottement des liquides* (Doctoral dissertation).
- Djeridi, H., Gabillet, C., & Billard, J. Y. (2004). Two-phase Couette-Taylor flow: arrangement of the dispersed phase and effects on the flow structures. *Physics of fluids*, 16(1), 128-139.
- Eckhardt, B., Grossmann, S., & Lohse, D. (2007). Torque scaling in turbulent Taylor-Couette flow between independently rotating cylinders. *Journal of Fluid Mechanics*, 581, 221-250.
- Farfán, R. F. M., Zambrano, T. Y. M., Sosa, V. M. D., & Zambrano, R. A. M. (2021). Design and construction of a thermoelectric system for high performance computers. *International Journal of Physical Sciences and Engineering*, 5(2), 25-33. <https://doi.org/10.29332/ijpse.v5n2.1359>
- Gazley Jr, C. (1958). Heat-transfer characteristics of the rotational and axial flow between concentric cylinders. *Transactions of the American Society of Mechanical Engineers*, 80(1), 79-89.
- Goldstein, S. (1937, March). The stability of viscous fluid flow between rotating cylinders. In *Mathematical Proceedings of the Cambridge Philosophical Society* (Vol. 33, No. 1, pp. 41-61). Cambridge University Press.
- Hubacz, R., & Wroński, S. (2004). Horizontal Couette-Taylor flow in a two-phase gas-liquid system: flow patterns. *Experimental thermal and fluid science*, 28(5), 457-466. <https://doi.org/10.1016/j.exptthermflusci.2003.07.004>
- Kadivar, E., el Moctar, O., & Javadi, K. (2018). Investigation of the effect of cavitation passive control on the dynamics of unsteady cloud cavitation. *Applied Mathematical Modelling*, 64, 333-356. <https://doi.org/10.1016/j.apm.2018.07.015>
- Kadivar, E., el Moctar, O., & Javadi, K. (2019). Stabilization of cloud cavitation instabilities using cylindrical cavitating-bubble generators (CCGs). *International Journal of Multiphase Flow*, 115, 108-125. <https://doi.org/10.1016/j.ijmultiphaseflow.2019.03.019>
- Kim, S. Y., & Cleaver, J. W. (1995). The persistence of drag reduction following the injection of microbubbles into a turbulent boundary layer. *International communications in heat and mass transfer*, 22(3), 353-357. [https://doi.org/10.1016/0735-1933\(95\)00026-U](https://doi.org/10.1016/0735-1933(95)00026-U)
- Kodama, Y., Kakugawa, A., Takahashi, T., & Kawashima, H. (2000). Experimental study on microbubbles and their applicability to ships for skin friction reduction. *International Journal of Heat and Fluid Flow*, 21(5), 582-588. [https://doi.org/10.1016/S0142-727X\(00\)00048-5](https://doi.org/10.1016/S0142-727X(00)00048-5)
- Lance, M., & Bataille, J. (1991). Turbulence in the liquid phase of a uniform bubbly air-water flow. *Journal of fluid mechanics*, 222, 95-118.
- Lathrop, D. P., Fineberg, J., & Swinney, H. L. (1992). Transition to shear-driven turbulence in Couette-Taylor flow. *Physical Review A*, 46(10), 6390.
- Lu, J., Fernández, A., & Tryggvason, G. (2005). The effect of bubbles on the wall drag in a turbulent channel flow. *Physics of Fluids*, 17(9), 095102.

Javadpour, S. M., Maryami, R., & Kadivar, E. (2022). Numerical study of frictional drag reduction using microbubbles in a vertical Couette-Taylor system. *International Journal of Physical Sciences and Engineering*, 6(1), 50-67. <https://doi.org/10.53730/ijpse.v6n1.4740>

- Lueptow, R. M., Docter, A., & Min, K. (1992). Stability of axial flow in an annulus with a rotating inner cylinder. *Physics of Fluids A: Fluid Dynamics*, 4(11), 2446-2455.
- Madavan, N. K., Deutsch, S., & Merkle, C. L. (1984). Reduction of turbulent skin friction by microbubbles. *The Physics of Fluids*, 27(2), 356-363.
- Mallock, A. (1896). III. Experiments on fluid viscosity. *Philosophical Transactions of the Royal Society of London. Series A, Containing Papers of a Mathematical or Physical Character*, (187), 41-56.
- Maryami, R., Farahat, S., & Mayam, M. S. (2014). Bubbly drag reduction in a vertical Couette–Taylor system with superimposed axial flow. *Fluid Dynamics Research*, 46(5), 055504.
- Maryami, R., Farahat, S., & Poor, M. J. (2015). The Effect of Small Bubbles on Resistance Reduction of Water Flow in Co-axial Cylinders with an Inner Rotating Cylinder. *Journal of The Institution of Engineers (India): Series C*, 96(2), 193-204.
- Maryami, R., Farahat, S., JavadPour, M., & Shafiei Mayam, M. (2015). Frictional drag reduction using small bubbles in a Couette-Taylor flow. *Journal of Marine Science and Technology*, 20(4), 652-669.
- Maryami, R., Javadpoor, M., & Farahat, S. (2016). Experimental investigation of head resistance reduction in bubbly Couette–Taylor flow. *Heat and Mass Transfer*, 52(12), 2593-2608.
- McCORMICK, M. E., & Bhattacharyya, R. (1973). Drag reduction of a submersible hull by electrolysis. *Naval Engineers Journal*, 85(2), 11-16.
- Mehel, A., Gabillet, C., & Djeridi, H. (2007). Analysis of the flow pattern modifications in a bubbly Couette-Taylor flow. *Physics of Fluids*, 19(11), 118101.
- Murai, Y., Fukuda, H., Oishi, Y., Kodama, Y., & Yamamoto, F. (2007). Skin friction reduction by large air bubbles in a horizontal channel flow. *International journal of multiphase flow*, 33(2), 147-163. <https://doi.org/10.1016/j.ijmultiphaseflow.2006.08.008>
- Murai, Y., Oiwa, H., & Takeda, Y. (2005). Bubble behavior in a vertical Taylor-Couette flow. In *Journal of Physics: conference series* (Vol. 14, No. 1, p. 018). IOP Publishing.
- Murai, Y., Oiwa, H., & Takeda, Y. (2008). Frictional drag reduction in bubbly Couette–Taylor flow. *Physics of fluids*, 20(3), 034101.
- Rust, A. C., & Manga, M. (2002). Effects of bubble deformation on the viscosity of dilute suspensions. *Journal of non-newtonian fluid mechanics*, 104(1), 53-63. [https://doi.org/10.1016/S0377-0257\(02\)00013-7](https://doi.org/10.1016/S0377-0257(02)00013-7)
- Sayyaadi, H., & Nematollahi, M. (2013). Determination of optimum injection flow rate to achieve maximum micro bubble drag reduction in ships; an experimental approach. *Scientia iranica*, 20(3), 535-541. <https://doi.org/10.1016/j.scient.2013.05.001>
- Shen, X., Ceccio, S. L., & Perlin, M. (2006). Influence of bubble size on micro-bubble drag reduction. *Experiments in Fluids*, 41(3), 415-424.
- Shiomi, Y., Kutsuna, H., Akagawa, K., & Ozawa, M. (1993). Two-phase flow in an annulus with a rotating inner cylinder (flow pattern in bubbly flow region). *Nuclear engineering and design*, 141(1-2), 27-34. [https://doi.org/10.1016/0029-5493\(93\)90089-R](https://doi.org/10.1016/0029-5493(93)90089-R)
- Sugiyama, K., Calzavarini, E., & Lohse, D. (2008). Microbubbly drag reduction in Taylor–Couette flow in the wavy vortex regime. *Journal of fluid mechanics*, 608, 21-41.
- Takeuchi, D. I., & Jankowski, D. F. (1981). A numerical and experimental investigation of the stability of spiral Poiseuille flow. *Journal of Fluid Mechanics*, 102, 101-126.
- Taylor, G. I. (1923). VIII. Stability of a viscous liquid contained between two rotating cylinders. *Philosophical Transactions of the Royal Society of London. Series A, Containing Papers of a Mathematical or Physical Character*, 223(605-615), 289-343.
- Van den Berg, T. H., Luther, S., Lathrop, D. P., & Lohse, D. (2005). Drag reduction in bubbly Taylor-Couette turbulence. *Physical review letters*, 94(4), 044501.
- van den Berg, T. H., van Gils, D. P., Lathrop, D. P., & Lohse, D. (2007). Bubbly turbulent drag reduction is a boundary layer effect. *Physical review letters*, 98(8), 084501.
- van Gils, D. P., Guzman, D. N., Sun, C., & Lohse, D. (2013). The importance of bubble deformability for strong drag reduction in bubbly turbulent Taylor–Couette flow. *Journal of fluid mechanics*, 722, 317-347.
- Wilcox, D. C. (2006). Turbulence modeling for CFD. La Canada, CA: DCW Industries. Inc, November.
- Wu, S. J., Hsu, C. H., & Lin, T. T. (2007). Model test of the surface and submerged vehicles with the micro-bubble drag reduction. *Ocean engineering*, 34(1), 83-93. <https://doi.org/10.1016/j.oceaneng.2005.12.010>

Xu, J., Maxey, M. R., & Karniadakis, G. E. (2002). Numerical simulation of turbulent drag reduction using micro-bubbles. *Journal of Fluid Mechanics*, 468, 271-281.

Biography of Authors

	<p>Seyed Morteza Javadpour He is an assistant professor of mechanical engineering at the University of Gonabad, Gonabad, Iran. He worked on the multiphase flows and cavitation phenomena for 10 years. Email: smjavadpour@Gonabad.ac.ir</p>
	<p>Reza Maryami He received his doctoral degree in 2016 from Yazd University. His research is concerned with multiphase and Couette-Taylor flows. Email: r.maryami@gmail.com</p>
	<p>Erfan Kadivar He is an Associate Professor at the Shiraz University of Technology, Iran. He completed his undergraduate studies in the Physics Study Program at the Faculty of Physics, Isfahan University. He continued his study in the Department of Physics at Isfahan University in 2006 with the field of Soft Condensed Matter. After that, he joined to Max Planck Institute for Dynamics and Self-Organization as a postdoctoral researcher. Currently, he is an Associate Professor of physics at the Shiraz University of Technology, Iran. Email: erfan.kadivar@sutech.ac.ir</p>